E. RELATIVISTIC HEAVY ION COLLISIONS

At the Relativistic Heavy-Ion Collider, RHIC, at Brookhaven National Laboratory, heavy ions collide at center-of-mass energies an order of magnitude higher than has previously been available anywhere. At these energies, it is expected that a baryon-free region of extremely high energy density will remain in the central region after the two colliding nuclei have passed through each other. It is believed that this situation will be more than sufficient to create a system of deconfined quarks and gluons - the "Quark Gluon Plasma". After formation, the plasma should expand and cool before passing into the normal hadronic phase that, in turn, expands further until the hadrons cease to interact with each other ("freezeout"). The important questions that need to be answered are: what are the direct probes and signatures of the plasma phase, and what identifiable traces of the quark-gluon phase remain in the observed hadronic final state? At ATLAS, our relativistic heavy ion group is involved in preparatory "fixed target" experiments at the Brookhaven AGS, and deeply involved in building and operating the PHOBOS experiment at RHIC.

e.1. The PHOBOS Experiment at RHIC

(B. B. Back, N. George, A. H. Wuosmaa, and the PHOBOS Collaboration - ANL, BNL, Krakow, MIT, NCU Taiwan, Univ. of Rochester, UIC, and Univ. of Maryland)

On June 12, 2000, the RHIC accelerator achieved its first Au + Au collisions, marking the beginning of a new era of relativistic heavy-ion research. Beginning in June, and throughout the run, which concluded in early September 2000, the PHOBOS experiment was actively recording and analyzing data. From early running the PHOBOS collaboration produced the first publication reporting[1] measurements from RHIC data, and analyses of data obtained during the Year 2000 physics run are now fully underway with a number of results released in preliminary form. 2000 has been a year of tremendous progress for the entire RHIC program, as well as the PHOBOS experiment. The current status of the experiment, data analyses and physics results for PHOBOS are discussed below.

The PHOBOS experiment focuses on measurements of hadronic observables for a large sample of events. The PHOBOS apparatus consists of a 4π multiplicity detector and two multi-particle tracking spectrometers capable of measuring and identifying particles with very low transverse momenta. The multiplicity detector provides event-by-event charged particle multiplicity distributions, which can be used to find interesting events for study in more detail using the spectrometers. The multiplicity distributions are interesting in their own right, and contain information on fluctuations and correlations, which relate to some of the proposed signatures of the plasma. The multiplicity distributions also contain information about the dynamic evolution of the collision.

An overall view of the PHOBOS apparatus as it was installed for the Year 2000 Physics run is shown in Fig. I-59; several different components are identified. The apparatus is effectively complete with the exception of some elements of one of the two tracking-spectrometer arms. The fabrication and installation of the multiplicity and vertex detectors was the responsibility of the groups at Argonne and UIC. Together, these systems contain over 22000 channels of silicon pad detector.

The Multiplicity detector provides event-by-event information on the charged particle multiplicity distributions over ± 5.4 units of pseudo-rapidity (η), with complete azimuthal coverage. The multiplicity measurement (see results below) is made using a centrally located, 11000 channel "Octagon" array of silicon pads supplemented with six 512 channel "Ring" counters placed up and down the beam pipe. These detectors measure the energy deposited as a function of angle with respect to the collision vertex.

The Vertex detector is designed to locate the position of the interaction vertex on an event-by-event basis. It is composed of two pairs of planes of silicon pad detectors, each plane segmented into 2048 channels so that the occupancy is low. Particles emitted from the collision vertex can be tracked by combining pairs of hits on the inner and outer Vertex planes such that the position of the reconstructed interaction point can be determined to a precision of better than $300\,\mu m$.

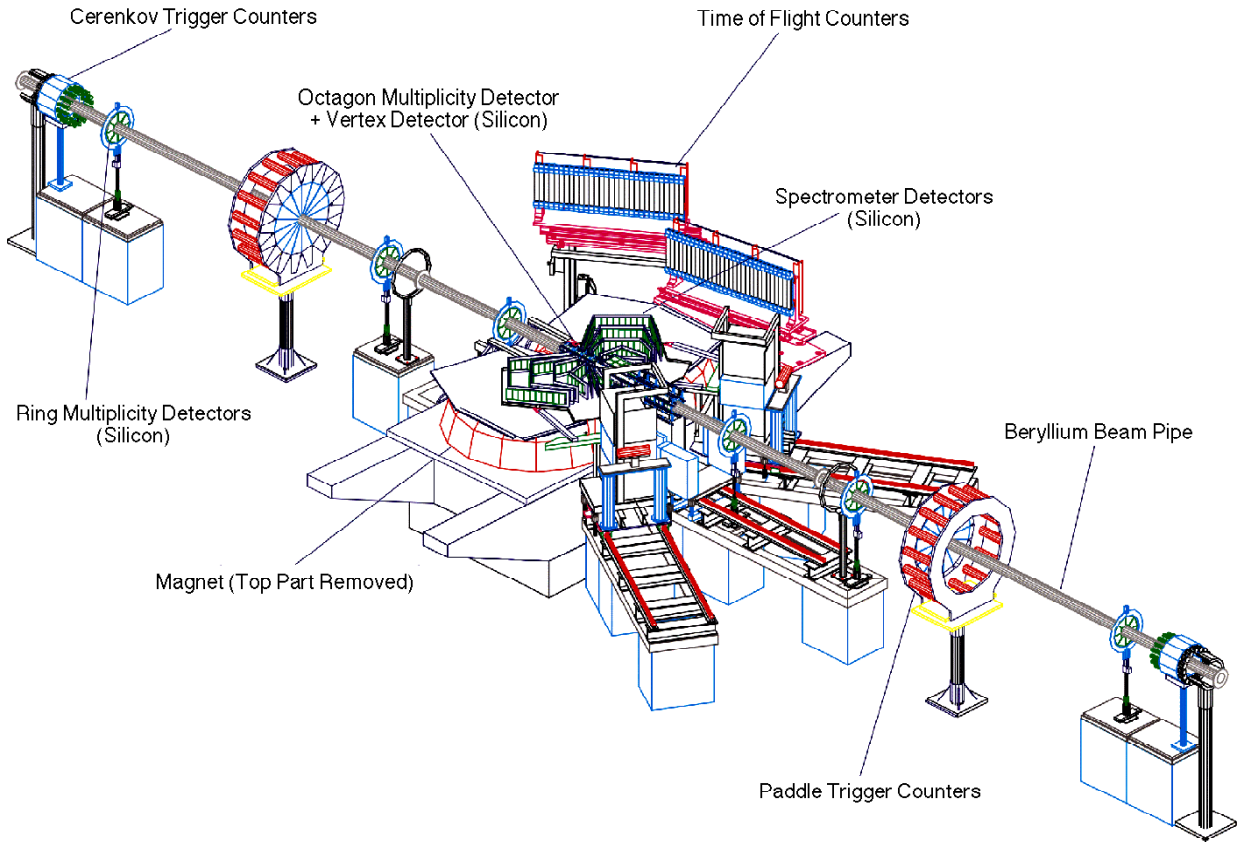

Fig. I-59. Overview of the PHOBOS experimental setup for the RHIC year 2000 running period. The top half of the spectrometer magnet has been removed for clarity.

Vertices are reconstructed over the entire range of the RHIC collision diamond, nominally corresponding to ± 20 cm about the center of the intersection region.

Installation and Testing of the Complete PHOBOS Detector

The full PHOBOS Year 2000 detector system was first installed in Dec. 1999 – Jan. 2000. During this period the readout and data-acquisition system were evaluated and cosmic-ray data were obtained in order to demonstrate the full functionality of the experiment. Following this evaluation period, the full detector was removed, and replaced with a limited subset of silicon sensors. This step was undertaken due to concerns about possible radiation damage to the sensitive front-end electronics and silicon detectors. This concern arose from results of the 1999 RHIC engineering run where poor beam conditions induced a condition known as CMOS latch-up in the front-end electronics chips. For the initial RHIC commissioning phase in 2000, 14 elements of the PHOBOS octagon multiplicity array, 6 elements of one tracking spectrometer arm, one quarter of the vertex detector, as well as a full complement of plastic scintillator trigger detectors were installed. A schematic diagram of the commissioning run setup appears in Fig. I-60. Despite this limited experimental arrangement, significant physics results were obtained from this commissioning run configuration (see below). Following the first Au + Au collisions on June 12 at an energy of $\sqrt{s_{NN}}$ = 56 GeV, the RHIC energy was increased to its full value for the year 2000 run, and first collisions at $\sqrt{s_{NN}}$ = 130 GeV were recorded on June 25. PHOBOS recorded physics data using the commissioning run setup at this higher energy as well.

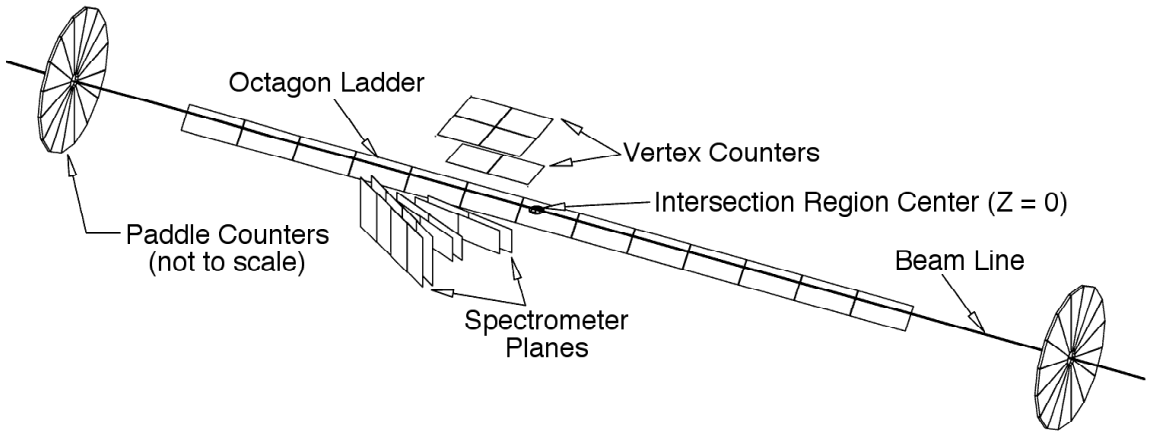

Fig. I-60. Schematic Diagram of the PHOBOS Year 2000 commissioning run setup (not to scale).

Following the successful conclusion of the commissioning period, the commissioning run configuration was removed from the RHIC tunnel and replaced with the full physics setup. This configuration consisted of the full complement of multiplicity detectors, including the octagon and ring detectors, one full tracking spectrometer arm, all detectors in the vertex finding arrays, trigger detectors, and the time-of-flight detectors.

Performance During the Year 2000 RHIC Physics Run

PHOBOS ran throughout the summer of 2000. During the commissioning period, a total of 6352 collisions were observed at $\sqrt{s_{NN}}$ = 56 GeV, and 12074 collisions at $\sqrt{s_{NN}}$ = 130 GeV. Following the commissioning phase, during which only 6 of a total of 57 bunches were circulated in the RHIC rings, the beam intensity was significantly increased, the beam optics were improved to increase the beam lifetime to as much as 8 hours, and the full complement of 57 bunches were injected into RHIC. At this point, significant luminosity was achieved at the full collision energy of $\sqrt{s_{NN}}$ = 130 GeV, and ultimately PHOBOS collected approximately 3.5 M collisions. Approximately 20% of these were obtained with the magnetic field turned off, and 40% with the magnet running at its full field value of 2 T with positive, and negative polarities, respectively. A total luminosity of 2.7 μb^{-1} was achieved, as measured with the two Zero-Degree Calorimeters (ZDCs) installed at PHOBOS. The details of event selection and triggering are discussed below.

Throughout the entire running period, frequent measurements of the noise and gain calibration of the entire PHOBOS system were taken to monitor the stability of the detectors. The noise, and hence the response of the detector were remarkably stable, with observed variations less than 2% throughout this period. The signal to noise ratio averaged over the entire setup was approximately 15 to 1. The variations in the measured gain response for this period were similarly small. The total fraction of non-functioning channels was less than 3% out of the total 95000 channels installed.

As discussed above, there were some concerns about possible radiation damage, as well as single-event-upsets, that could affect the performance of the silicon pad detectors and their Front-end electronics (FEE). A fast-responding circuit designed to sense the so-called “latchup” behavior, and protect the FEE chip, was installed for all silicon sensors in the experiment. This latchup protection circuit worked well during the run, although only a few instances of this behavior were observed. At the end of the run, no damage to the either the detectors or their electronics as a result of radiation exposure was observed.

During RHIC running, events were triggered in PHOBOS using the two sets of plastic scintillator counters. Triggers were derived from the timing characteristics of data from the trigger counters; the time of arrival of particles in each set of counters was measured, and for events where this time difference was less than 38 ns the full data-acquisition system was triggered. This rather broad time window included events from background (beam-gas or beam-beamline) interactions, as well as from true collisions. Events with a time difference of less than 3 ns were

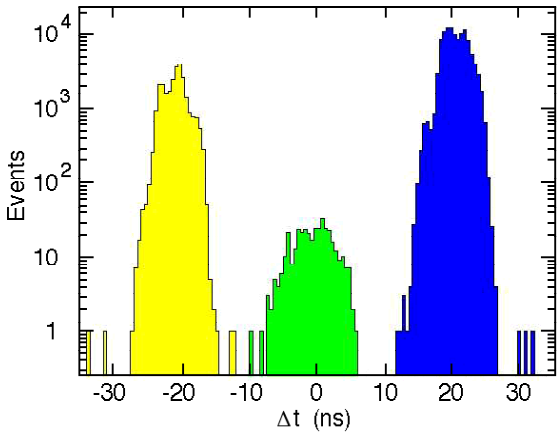

Fig. I-61. PHOBOS trigger timing spectrum, showing collisions at $\sqrt{s_{NN}}$ = 56 GeV.

considered to be good collisions. A timing spectrum from the first collisions at $\sqrt{s_{NN}}$ = 56 GeV appears in Fig. I-61; the true collisions appear near Δt = 0 ns, and the impact parameter of the collision, as well as the number of participating nucleons N_{part}, we analyze the energy-loss data from the trigger detectors. As most of the particles passing through the paddle counters are minimum ionizing, the sum of the energy loss measured in the paddle counters is a measure of how many particles are detected. To estimate the centrality, the response of the paddle counters was studied using a Monte-Carlo simulation. From the results of the simulation, we can extract a direct relationship between the measured paddle sum-energy signals, and the number of nucleons participating in the collision, as illustrated in Fig. I-62. From this determination, we deduce that the approximate number of nucleons participating in the collision is N_{part} = 343 at $\sqrt{s_{NN}}$ = 56 GeV, and N_{part} = 356 at $\sqrt{s_{NN}}$ = 130 GeV. This information was used in the subsequent physics analyses as described below.

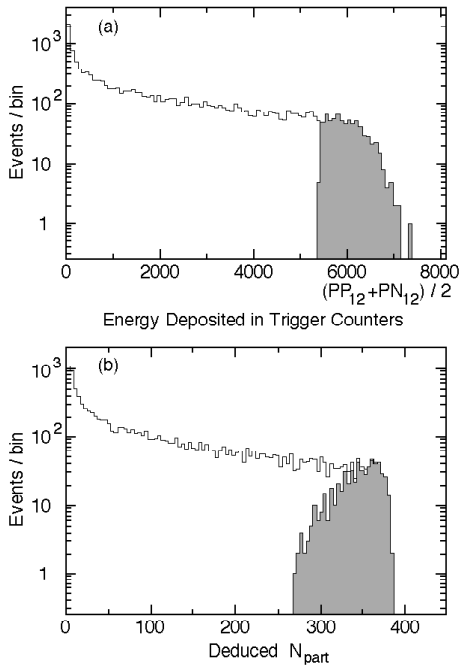

Fig. I-62. (a) Paddle sum-energy spectrum. The shaded area corresponds to the 6% most central collisions. (b) Yield vs. number of participants from Monte Carlo simulations. The shaded region corresponds to the range ofparticipants corresponding to the 6% region in (a).

The position of the collision vertex – the point in space at which the Au ions actually collide – was determined using particle tracks recorded in the vertex detectors, as well as in the two particle tracking spectrometers. Figure I-63 shows tracks recorded from a collision taken during the commissioning run period. All of the reconstructed tracks point back to the same point in space within approximately 300 μm. For the commissioning period, due to the limited number of detectors installed, the vertex detectors were not used to identify the vertex. Once the vertex had been identified, however, data in the vertex detectors were used for actual physics measurements (see below).

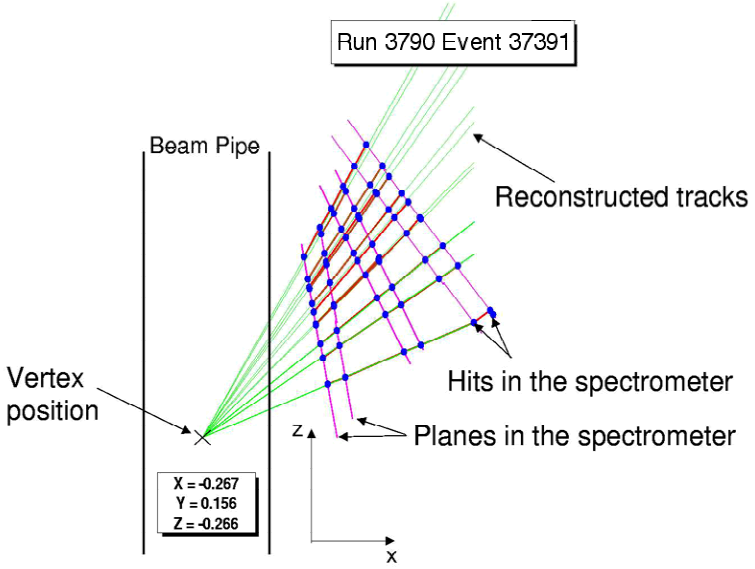

Fig. I-63. Event diagram showing reconstructed tracks observed in the PHOBOS commissioning run tracking spectrometer.

With the full physics configuration of PHOBOS, both of the tracking spectrometers, as well as the fully installed vertex detectors were used to provide complementary determinations of the vertex position. Figure I-64 shows a vertex identification spectrum from the vertex tracker detectors for a single event at $\sqrt{s_{NN}}$ = 130 GeV. The histogram shows the projections of all possible combinations of hits in the inner, and outer layers of the vertex tracker onto the nominal beam axis. The sharp spike at z = 0cm, where z denotes the distance from the center of the experiment along the nominal beam axis, corresponds to the actual vertex position. The vertex finding precision of the different methods was better than 200 μm in z. Finally, Fig. I-65 shows the distribution of reconstructed collision vertices as a function of z. The cutoff in the spectrum near z = +20 cm arises from the edge of the tracking spectrometer acceptance. With the focusing magnets instrumented in the PHOBOS interaction region, the collisions were spread throughout a rather broad range of z. Most of the physics results discussed below were taken from events with a reconstructed vertex within 10 to 20 cm of the nominal center of the apparatus. With improved focusing in 2001 it is expected that the collision diamond will be much more closely confined to near z = 0, and a much higher fraction of triggered events will have vertices within the optimal zone.

Physics Results from the Year 2000 Physics Run

dNch/dη at mid-rapidity:

The most straightforward observable quantities from energetic heavy-ion collisions involve the number and distribution of the emitted charged particles. These quantities are of particular interest as they are sensitive to all processes contributing to particle production, and serve as measures of the energy, and entropy densities achieved during the collision. The PHOBOS experiment has a number of elements designed to study the charged-particle multiplicity.

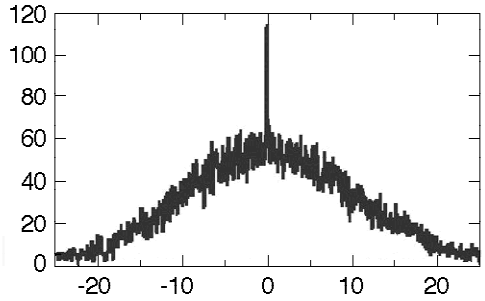

Fig. I-64. Vertex identification plot for one Au + Au collision at 130 GeV.

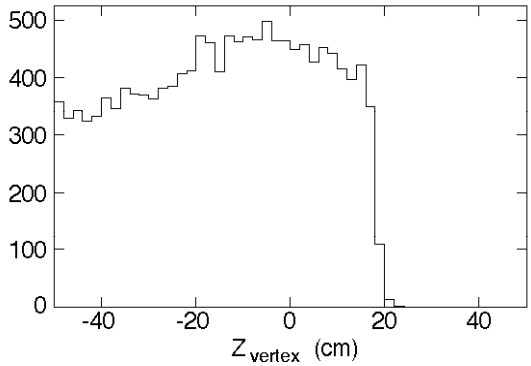

Fig. I-65. Vertex distribution from Au + Au collisions at 130 GeV. A reconstructed vertex in both spectrometer and vertex detectors is required. The cutoff at z = 20 cm reflects the end of the spectrometer acceptance.

The first measurements of charged particle production from relativistic Au + Au collisions at RHIC were reported from the PHOBOS experiment,[1] from data obtained during the commissioning phase of RHIC running in June 2000. The events were selected as described above. The first measurements were confined to the most central collisions, for particles emitted in the mid-rapidity region ($|\eta| < 1$). The values obtained here are particularly sensitive to the initial energy and entropy densities in the collisions, as suggested by Bjorken.[2] The pseudo-rapidity density was determined by counting "tracklets" – tracks measured in the partial spectrometer arm or vertex detector that connect either hits in two of the 6 spectrometer planes, or the two vertex detector planes, with the reconstructed vertex position. After corrections are applied for detector acceptance, and the effects of secondary particle production and combinatorial background, the pseudo-rapidity density $dN_{ch}/d\eta(|\eta| < 1)$ can be determined. For the 6% most central collisions, the measured values are $dN_{ch}/d\eta$ = 408 ± 12 (stat) ± 30 (syst), and 555 ± 12 (stat) ± 35 (syst), at $\sqrt{s_{NN}}$ = 56, and 130 GeV, respectively.

Figure I-66 shows the measured charged-particle pseudo-rapidity density at mid rapidity for the 6% of the most central collisions, divided by the number of nucleon pairs participating in the collision (N_{pp} = 1/2 N_{part}). For comparison, data points from p-p collisions[3] at the ISR, and from Pb + Pb collisions[4] from the CERN SPS program are shown. A number of interesting points can be made. First, the number of produced charged particles scaled by the number of participant pairs increases by approximately 30% going from $\sqrt{s_{NN}}$ = 56 to 130 GeV. Furthermore, compared to the yield observed from $\bar{p}$-p collisions, the charged particle production is enhanced by nearly 40%, clearly indicating some collective effects unique to the heavy-ion system. Finally, the yield per participant pair is some 70% larger than that observed in lower energy Pb + Pb collisions at the SPS, indicating a corresponding increase in the initial energy density achieved in the Au + Au collisions.

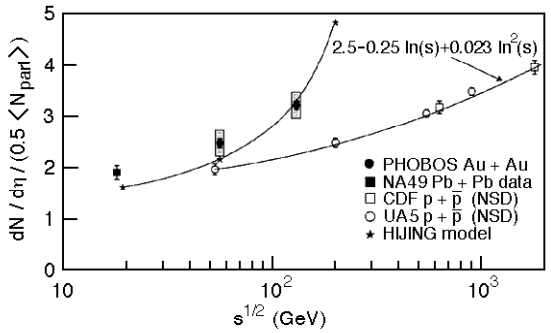

Fig. I-66. Plot of the measured pseudo-rapidity density from PHOBOS (solid circles). Also plotted is the prediction of HIJING (stars), and data from p-p scattering (open symbols). The result from Pb + Pb scattering at the CERN SPS are is shown as the solid square.

A number of theoretical predictions were available for this observable. The stars joined by the solid curve in Fig. I-66 represent the prediction of the HIJING event generator[5] for $dN_{ch}/d\eta$ at $\eta = 0$. This prediction is in apparent good agreement with the data. A calculation using very different physics assumptions including the effects of parton saturation[6], however, predicts very similar results for $dN_{ch}/d\eta(\eta = 0)$. In order to distinguish between these two models, more detailed measurements are required. For example, the saturation and HIJING models predict significantly different centrality dependences for $dN_{ch}/d\eta$. HIJING predicts that $dN_{ch}/d\eta$ scales approximately linearly with N_{pp}, with particle production arising from a combination of soft, non-perturbative processes, and hard perturbative scattering interactions. The saturation model, however, predicts a roughly constant centrality dependence. Limited statistics precluded extraction of the centrality dependence of $dN_{ch}/d\eta$ from the commissioning run data, but it is now possible to study this dependence with the much more substantial data set obtained from the Year 2000 physics run.

Centrality dependence of $dN_{ch}/d\eta$ at $\eta = 0$:

A similar tracklet analysis was performed for the $\sqrt{s_{NN}}$ = 130 GeV data obtained during the 2000 Physics run, using data from the two tracking spectrometer arms, as well as the fully instrumented vertex detector. The event selection, as well as the determination of the number of participating nucleons, was as described above. Figure I-67 shows the preliminary results of this analysis, with the measured $(dN_{ch}/d\eta)/(0.5 \times N_{part})$ plotted versus the number of participating nucleons N_{part}. The systematic uncertainty of approximately 6% was determined by comparing the results from the different detector systems. Also plotted are the predictions from the HIJING and saturation models. The data do not support either of the theoretical predictions, and in fact fall somewhere in between the two. Still other calculations based upon either a Glauber description of the collisions with particle production described by a modified wounded nucleon prescription, or by a model that divides the particle production into a soft, non-perturbative part which scales by the number of participants and a hard scattering component that scales with the number of nucleon-nucleon collisions, are in better agreement with the data.[7]

$dN_{ch}/d\eta$:

Further information may be obtained by studying the pseudo-rapidity dependence of $dN_{ch}/d\eta$. This measurement was performed using the multiplicity detectors that were constructed by the Argonne-UIC group. This multiplicity measurement is completely independent of the tracklet analyses described above. To study $dN_{ch}/d\eta(\eta)$, hits in the multiplicity octagon and ring detectors were analyzed. In order to account for the occupancy of the detector for events with large numbers of produced charged particles (where more than one particle traverses a single pad in the multiplicity detector) the average occupancy of the detector for selected bins of centrality and pseudorapidity were determined by assuming that the population of any given pad was determined by Poisson statistics. That assumption was then fit to the measured number of occupied, and unoccupied pads. The observed average number of particles going through a given occupied pad was as large as 1.6 for very central collisions at mid rapidity. In order to take

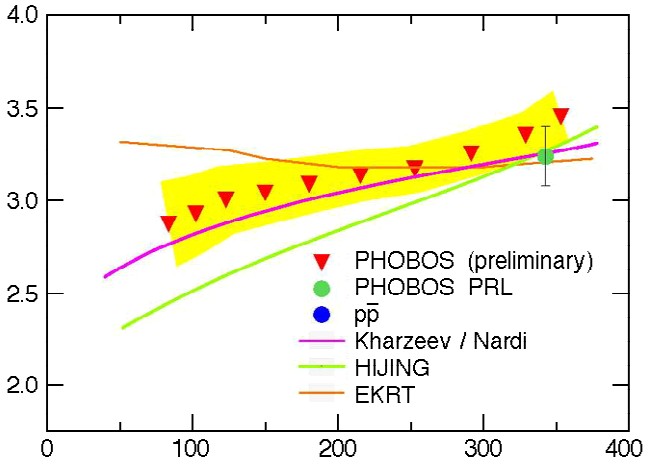

Fig. I-67. Centrality dependence of $dN_{ch}/d\eta/(0.5XN_{part})$ from PHOBOS (preliminary results). Also shown are the predictions of HIJING[5] (solid curve), saturation model,[6] and the Karzeev and Nardi prescriptions[7] (dot-dashed curve).

account of other effects such as secondary particle production, weak particle decays, and absorption of low-momentum particles in the beam pipe, comparisons to the predictions of Monte Carlo simulations were employed. The measured distributions of $dN_{Ch}/d\eta$ at $\sqrt{s_{NN}}$ = 130 GeV for several centrality bins appear in Fig. 1-68, with histograms that represent the predictions of HIJING. The observed distributions are, in all cases, wider than those predicted by HIJING. One possibility is that the effects of hadronic rescattering or final-state interactions may play a role beyond the central plateau region ($|\eta| > 2$). These effects are not included in HIJING. Some indications that this may be the case come from a comparison of the data for the most central bin with the predictions of the AMPT model[8] that includes particle production mechanisms similar to HIJING, but describes the hadronic final state with a hadronic cascade model. The prediction is in much better agreement with the data, and further investigations in this direction would be most interesting.

Baryon density at mid rapidity:

One prediction of the situation achieved in heavy-ion collisions at highly relativistic energies is that the two nuclei pass through each other, leaving a very hot, but essentially baryon free, region between them from which particles and anti-particles are produced. In order to determine whether this central region is actually baryon-free, it is useful to study the ratio of anti-baryons to baryons at mid-rapidity. If the participant baryons carried within the colliding nucleons are indeed swept out of the hot central zone, then the ratio of the numbers of observed baryons, and anti-baryons at mid-rapidity should be approximately unity. Furthermore, this ratio may be related to the amount of kinetic energy transformed into energy available for particle production.

The ratio of anti-protons to protons at mid rapidity was measured in PHOBOS using data from the tracking spectrometer with the magnet energized to its full field value of 2T. Tracks were analyzed by first identifying straight tracks in the 6 spectrometer planes within the field-free region near the beam pipe. These tracks were followed into the magnetic field region and then momentum analyzed by comparing hits in the remaining spectrometer planes with predetermined patterns in a look-up table. The particles were identified by a measurement of their differential energy loss in the spectrometer planes. Figure I-69 shows a particle identification spectrum for tracks corresponding to negatively charged pions, kaons and protons ($\bar{p}$). In order to address systematic uncertainties, data obtained with the two magnet polarities were compared. The different acceptances for positively and negatively charged species obtained with the two polarities effectively cancel. The measured value of $\bar{p}/p$ was R = 0.54 ± .05(stat) ± .05(syst). The fact that this ratio is somewhat less than one implies that the mid-rapidity region is not yet entirely baryon free. The measured value is, however, approximately six times larger than that observed in Pb + Pb collisions at the SPS. The $\bar{p}/p$ ratio is expected to more closely approach unity as the collision energy is increased to $\sqrt{s_{NN}}$ = 200 GeV in the RHIC 2001 physics run.

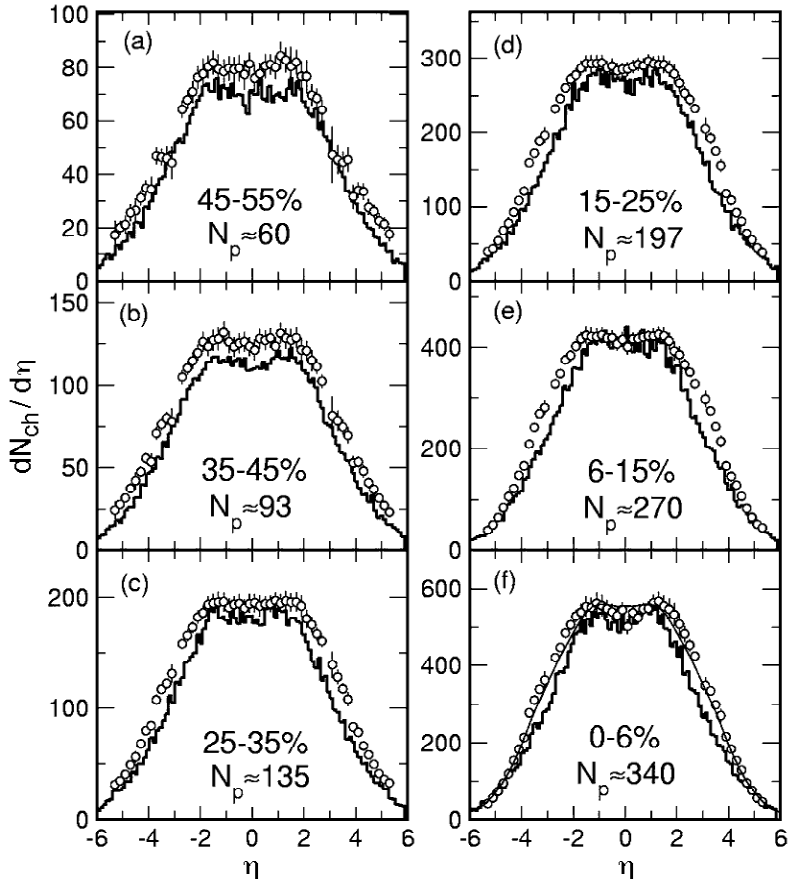

Fig. I-68. Preliminary charged-particle pseudo-rapidity density distributions for several different collision centralities, as measured by PHOBOS for $\sqrt{s_{NN}}$ = 130 GeV collisions (data points). The histograms correspond to the predictions of HIJING, and the solid curve in (f) represents the predictions of the AMPT model.

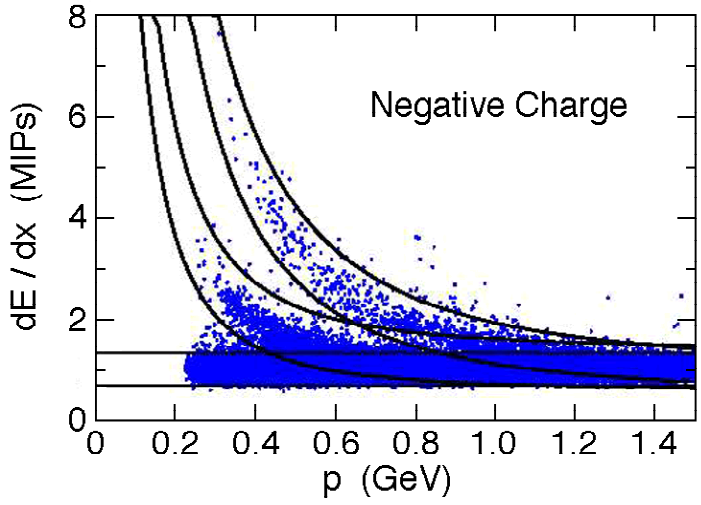

Fig. I-69. Particle identification spectrum showing identified π^-, K^-, and p .

Elliptic flow:

When the two colliding Au nuclei overlap, there is briefly a period of extremely high density and intense compression within the collision zone. Pressure gradients that build up within this region may manifest themselves in the distributions of emitted charged particles, or in the distributions of their momenta. The degree to which this may occur depends upon the centrality of the collision, the equation of state of the nuclear matter, and possibly the properties of the hot zone left over after the nuclei pass through one another. For non-central collisions, the collision zone takes on an azimuthally asymmetric shape, similar to an almond or a football, with the degree of eccentricity determined by the degree of overlap. The phenomenon of elliptic flow occurs when the asymmetry of this collision zone is reflected in the azimuthal asymmetry of the distributions of particles or their momenta when measured with respect to the plane of the reaction.

In order to measure elliptic flow in PHOBOS, first the reaction plane is determined by the usual sub-event technique, where the azimuthal particle distributions $dN_{ch}/d\phi$ for half of the particles is fit to determine a reaction plane angle ϕ_0. Afterwards, the azimuthal angular distribution with respect to that reaction plane of the remaining particles is determined. To extract the elliptic flow signal, the angular distribution with respect to the reaction plane is fit to the expression $dN_{ch}/d\phi = A(1 + v_2\cos2*(\phi - \phi0))$. A plot showing the experimental azimuthal angular distributions at $\sqrt{s_{NN}}$ = 130 GeV appears in Fig. I-70 for different impact parameters. For very central collisions, there is little or no asymmetry in the overlap zone and consequently no discernable flow signal. For peripheral collisions, however, there is a clear asymmetry corresponding to a significant flow signal. Preliminary indications are that the size of the observed flow signal may be comparable to that which is expected from hydrodynamical calculations.

Status and Schedule

The current status of PHOBOS for 2001 is excellent. The elements of the experiment not in place for the year 2000 running, specifically, the elements of the second tracking spectrometer arm, are now complete and awaiting installation at Brookhaven. Due to the absence of any observable adverse effects from radiation damage, the existing detector is immediately ready to take data once collisions are achieved in 2001. Furthermore, the data-acquisition system was upgraded to improve that data throughput by a factor of approximately 4. This upgrade has included implementation of a Gigabit Ethernet link, additional processors in the Mercury zero-suppression system, and an upgrade to the main data acquisition computer. All of these upgrades are in place and operational.

Beyond 2001, discussions are underway for a possible upgrade to the PHOBOS apparatus to study the production of open charm, through the observation of high momentum electrons arising from D-meson decays. This upgrade would include the addition of a high-resolution micro-vertex detector capable of observing particles emanating from displaced vertices, and electron identification through a combination of transition-radiation detectors and electro-magnetic calorimeters.

1B. B. Back *et al.*, Phys. Rev. Lett. **85**, 3100 (2000).
2J. D. Bjorken, Phys. Rev. D **27**, 140 (1983).
3F. Abe *et al.*, Phys. Rev. D **41**, 2330 (1990).
4J. Bachler *et al*., Nucl. Phys. **A661**, 45 (1999).
5X. N. Wang and M. Gyulassy, Phys. Rev. D **44**, 3501 (1991).
6K. J. Eskola *et al*., Nucl. Phys. **B570**, 379 (2000).
7D. Karzheev and M. Nardi, Preprint nucl-th/0012025.
8Z. Lin *et al*., Preprint nucl-th/0011059.

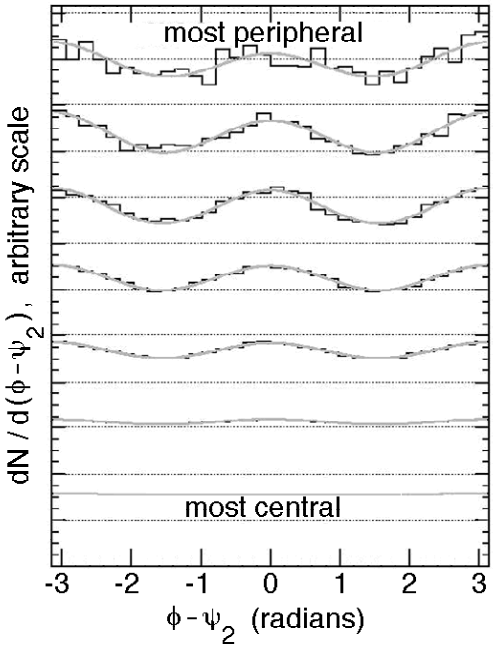

Fig. I-70. Preliminary azimuthal distributions of particle measured for different collision centralities. The pronounced asymmetry for peripheral collisions is a clear signature of elliptic flow.

e.2. Studies of Au + Au Collisions at 6, 8, 10.8 GeV/Nucleon at the AGS

(E917 collaboration: B. B. Back, A. Gillitzer, W. F. Henning, D. J. Hofman, V. Nanal, A. Wuosmaa, R. R. Betts,* W. C. Chang,‡ C. Y. Chi,†† Y. Y. Chu,† J. B. Cumming,† J. C. Dunlop,§ W. Eldredge,‡ S. Y. Fung,‡ R. Ganz,* E. J. Garcia-Solis,|| G. Heintzelman,§ B. Holzman,* J. H. Kang,¶ E. J. Kim,¶ S. Y. Kim,¶ Y. Kwon,¶ D. McLeod,* A. C. Mignerey,|| M. Moulson,†† C. A. Ogilvie,§ R. Pak,** A. Ruangma,|| D. E. Russ,|| R. Seto,‡ P. J. Stankas,|| G. S. F. Stephans,§ H. Q. Wang,‡ F. Wolfs,** H. Xiang,‡ G. Xu,‡ H. B. Yao,§ and C. Zou‡)

Introduction

Collisions of Au + Au nuclei at relativistic energies were studied by the E917 collaboration at the AGS accelerator at Brookhaven National Laboratory at beam energies of 6, 8, and 10.8 GeV/nucleon. The purpose of this experiment was to study the general properties of the hot fireball produced in these collisions via measurements of identified particle spectra over a wide angular region. In the analysis, particular interest was devoted to the analysis and interpretation of both the proton, pion, kaon, ϕ-mesons, Λ, and their anti-particles, Several aspects of these studies were published previously Ref. 1,2,3 and will not be discussed here. Recently, we completed the analysis and interpretation of the proton spectra (Ref. 4) and the ratio $\bar{\Lambda}$ to $\bar{p}$ (Ref. 5) which will be described below.

Experiment

The experimental arrangement consists of a magnetic spectrometer which allows for momentum analysis of particles emerging from the target. Particle trajectories are tracked by several multiwire ionization chambers located both in front and behind the magnet. The time-of-flight wall provides particle identification when combined with the measured particle momentum.

Several beam counters located upstream of the target provide timing and trajectory information on each beam particle. When combined with the spatial location of

the projectile remnant at the Hodoscope it is possible to determine the orientation of the reaction plane, with reasonable accuracy. The centrality of the collision (impact parameter) is obtained either by observing the multiplicity of particles (mostly pions) in the New Multiplicity Array (NMA) or the total energy of the projectile remnant in the Zero Degree Calorimeter (Z_{cal}).

Proton Spectra – Stopping

Nuclear matter is believed to be compressed to high baryon density ρ_B in central collisions of heavy nuclei at relativistic energies. In the interaction region of the colliding nuclei, nucleons undergo collisions which reduce their original longitudinal momentum. This loss of rapidity is an important characteristic of the reaction mechanism, and is often referred to as stopping. Relativistic heavy-ion collisions are unique in the sense that secondary collisions of excited baryons are expected to contribute to the rapidity loss leading to simultaneous stopping of many nucleons within the interaction volume. The baryon density reached may thus be large enough to induce phase transitions, such as quark de-confinement. The observation of large numbers of baryons at mid-rapidity is indicative of compression to high baryon density, but the quantitative estimate of the densities reached during the collision is only possible via model calculations. However, an important key to our understanding of this phenomenon is the availability of systematic data on the rapidity distributions of baryons over a broad range of conditions, such as beam energy and centrality.

In the E917 experiment we studied proton rapidity distributions from Au + Au collisions at 6, 8, and 10.8 GeV/nucleon as a function of centrality. At these energies, the measured ratio of antiprotons to protons is very small (< 0.03%) and the production of protons from Λ-decay contributes less than 5% to the total yield. The measured protons are therefore expected to directly reflect the distribution in rapidity of the initial baryons (assuming that the neutron rapidity distribution has a similar shape). The measured rapidity distributions at all three beam energies are shown in Fig. I-71.

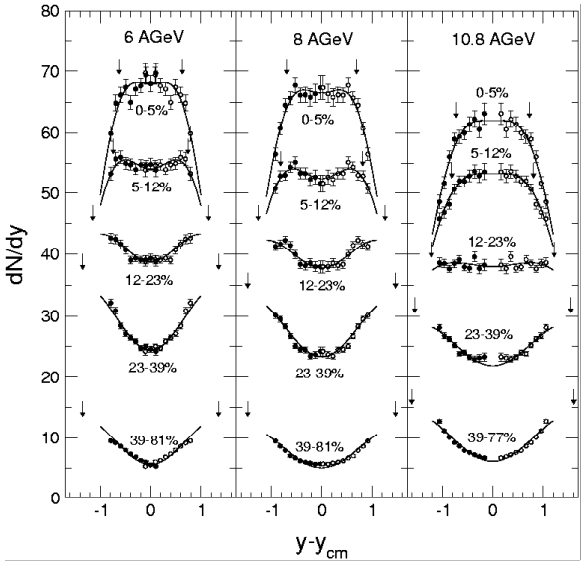

Fig. I-71. Proton rapidity distributions for all centrality classes at all three beam energies from Boltzmann fits to the invariant cross sections. The open symbols are the data reflected about mid-rapidity. The errors are statistical only. The curves represent double Gaussian fits to the data (see text), the centroids of which are indicated by the arrows.

They exhibit a similar evolution with centrality and are clearly bimodal in shape for peripheral collisions and change to shapes, which for central collisions may still be bimodal in nature. This suggests that the degree of stopping in central collisions is not complete, even in this heavy system.

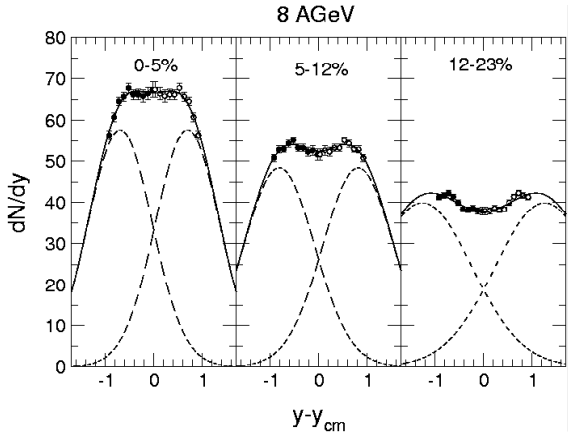

Fig. I-72. Fits to the proton dN/dy distributions for the three most central event classes at 8 GeV/nucleon illustrating the evolution of shape with centrality. The solid curves are the sums of two individual Gaussians (dashed curves).

The centrality dependence of the rapidity density at each beam energy is shown in Fig. I-72. The data are shown relative to the rapidity of the center-of-mass of the system y_{cm} which equals 1.35, 1.47, and 1.61 for beam kinetic energies of 6, 8, and 10.8 GeV/nucleon, respectively. The data points reflected about mid-rapidity are shown as open symbols. The errors were calculated from the fitting procedure. The present values of dN/dy for the most central event class at 10.8 GeV/nucleon are in good agreement with the previously reported values from the E866 Collaboration.

For each beam energy, a common trend is observed in the evolution of the shape of the rapidity distributions as a function of centrality. For the most peripheral event class the distribution has a minimum value of dN/dy ~ 6 at mid-rapidity. This concave shape persists to the next most central event class, corresponding to a centrality cut of (23-39)%, consistent with the expectation that most of the participant protons reside at beam rapidities following these relatively peripheral collisions. For more central collisions, the rapidity distributions become progressively flatter, and begin to develop a broad maximum at mid-rapidity for all beam energies. The trend of the data suggests, however, that for the most central collisions, the distribution does not evolve to a single peak centered at mid-rapidity, but rather is consistent with two components each displaced from mid-rapidity, or with a set of sources spread throughout the rapidity range. To qualitatively emphasize this point, we fit each of the measured distributions with two Gaussian peaks centered symmetrically about mid-rapidity. These are shown superimposed on the data for the three most central event classes at 8 GeV/nucleon in Fig. I-72 and clearly display the trend. This result, somewhat surprisingly, implies that complete stopping is not achieved at AGS energies and that the longitudinal rapidity distribution is a result of transparency.

These distributions thus show a consistent evolution with increasing energy and centrality leading to maximal rapidity loss for the most central collisions and the highest energy. This result suggests the importance of secondary reactions in the heavy-ion case, contrary to the situation in p + A collisions. Nevertheless, the degree of stopping of the incident baryons is far from complete and only a fraction of the observed protons can be accounted for by the emission from a stopped isotropically emitting source. The remainder still possess considerable longitudinal momentum. It is not possible to say unequivocally from the present data alone whether or not this corresponds to a situation where the colliding nuclei are, to some extent, "transparent", or a fully stopped and compressed system has re-expanded. However, the systematic behavior of the centrality dependence of the shapes of the rapidity distributions suggests, surprisingly, that the former is the case.

$\bar{\Lambda}$ and $\bar{p}$ Production

Enhanced antimatter and strangeness production have both been proposed as signatures of the phase transition to the quark-gluon plasma (QGP).[6-8] Strange

antibaryons combine both of these signatures in a single production channel, and may prove particularly sensitive to the formation of the QGP. Of particular interest is the ratio $\bar{\Lambda}/\bar{p}$, which reflects the relative abundance of anti-strange quarks to light antiquarks.

However, both $\bar{\Lambda}$ and $\bar{p}$ are also produced when the collision is purely hadronic. Hadronic matter with sufficient scattering can reach a chemical equilibrium containing the full spectrum of known hadrons. Equilibrated chemical models of heavy-ion collisions are generally able to reproduce the measured ratios of total yields of particles such as pions and kaons. Such models predict values for the $\bar{\Lambda}/\bar{p}$ ratio in the range 0.15-0.9 at AGS beam energies.[9,10] A thermal model analysis that accounts for the measured K^+/p^+ and K^+/K^- ratios gives a most probable value of $\bar{\Lambda}/\bar{p} = 1$.

Enhanced antibaryon production may also be produced by many-body collisions between pions, e.g. $np \rightarrow \bar{p} + p$. The rate of antibaryon production can be estimated from the inverse annihilation $\bar{p} + p \rightarrow np$. Calculations indicate that a significant number of both $\bar{\Lambda}$ and $\bar{p}$ may come from these processes, but it is not yet clear how to incorporate these many-body collisions into current hadronic cascade calculations.

In summary hadronic models predict $\bar{\Lambda}/\bar{p}$ $\bar{\Lambda}/\bar{p} < 1$, with extreme possibilities on the order of 1.5. Thus the experimental detection of a $\bar{\Lambda}/\bar{p}$ ratio significantly larger than unity may signal the breakdown of these hadronic models, and possibly the onset of non-hadronic degrees of freedom in the system. Of particular interest is the centrality dependence of the $\bar{\Lambda}/\bar{p}$ ratio, which may discriminate between the various models attempting to describe antibaryon production: QGP, hadronic scattering, and thermal models.

In experiment E917 we therefore measured the $\bar{\Lambda}$ and $\bar{p}$ production rate in Au + Au collisions at 10.8 AGeV beam energy. The invariant spectra and yields were measured for both species in central and peripheral collisions.

The transverse mass spectra are shown in Fig. I-73.

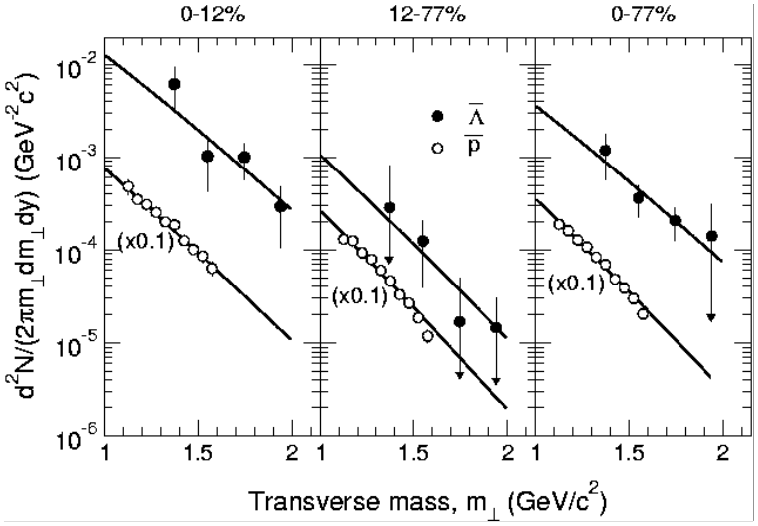

Fig. I-73. Invariant spectra as a function of transverse mass for $\bar{\Lambda}$ (solid circles) and $\bar{p}$ (open circles, multiplied by 0.1 for clarity) in three centrality classes. The error bars include 2% point-to-point systematic error. The solid lines are from the simultaneous fit to the $\bar{\Lambda}$ and $\bar{p}$ spectra as described in the text.

Since the $\bar{p}$ spectra have a strong contribution from $\bar{\Lambda}$ decays, it is advantageous to perform a simultaneous fit to both spectra in order to obtain the most accurate measure of the $\bar{\Lambda}/\bar{p}$-ratio. In a Monte Carlo study we found that the spectra of $\bar{p}$'s from the $\bar{\Lambda}$ decays exhibit a Boltzmann shape with an inverse slope, which is reduced to about 84% of that for the original $\bar{\Lambda}$ and an integrated yield reflecting the 64% branching ratio for the $\bar{\Lambda} \rightarrow p^+$ decay. The $\bar{\Lambda}$ and $\bar{p}$ transverse mass spectra were therefore fit simultaneously using the functions

$$\frac{1}{2\pi m_\perp}\frac{d^2N_{\bar\Lambda}}{dm_\perp dy}=\frac{dN_{\bar\Lambda}}{dy}B(T_{\bar\Lambda})$$

$$\frac{1}{2\pi m_\perp}\frac{d^2N_{\bar p}}{dm_\perp dy}=\frac{dN_{\bar\Lambda}}{dy}\left(\frac{B(T_{\bar p direct})}{(\bar\Lambda/_{\bar p direct})}\right)+0.639B(T_{\bar p direct})$$

respectively. The parameters obtained from this fitting procedure, namely the $\bar\Lambda$ yield, dN($\bar\Lambda$)/dy, the ratio of $\bar\Lambda$'s to directly produced $\bar p$'s, ($\bar\Lambda/\bar p$ direct), the inverse slope of the $\bar\Lambda$ spectrum, T($\bar\Lambda$) and the inverse slope of the directly produced $\bar p$, T($\bar p$). Of particular interest is the $\bar\Lambda/\bar p$direct ratio which is found to increase from $0.26^{+0.19}_{-0.15}$ in peripheral collisions (12-77%) to $3.6^{+4.7}_{-1.8}$ in central collisions (0.12%) and attain an average value of $1.3^{+0.6}_{-0.4}$ when integrated over the centrality (0-77%) of the interaction cross section.

These results represent the first direct measurement for Au + Au collisions at AGS energies, but they are in good agreement with earlier measurements in the Si + Au system as well as an earlier indirect estimate obtained by comparing $\bar p$ yields in two experiments, E864 and E878, with different acceptance, as illustrated in Fig. I-74.

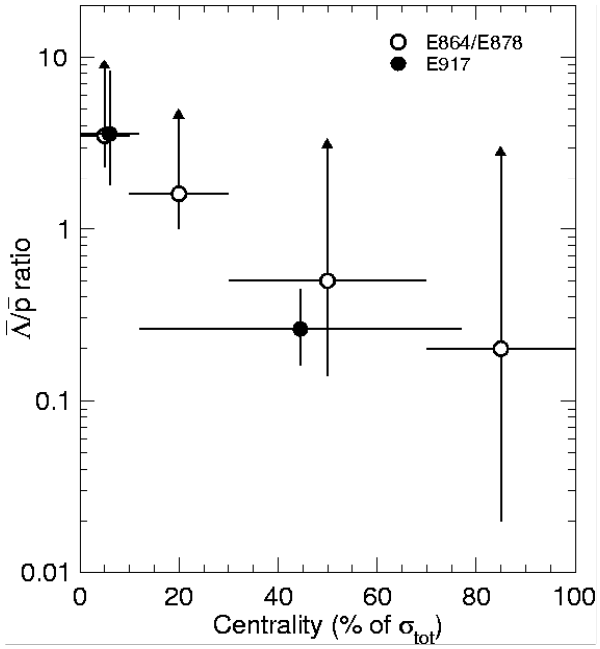

Fig. I-74. The $\bar\Lambda/\bar p$-ratio is shown as a function of the centrality given in terms of the percentage of the total interaction cross section. The E917 data are shown as solid circles with 1s statistical error bars for the $\bar\Lambda/\bar p$-ratio. The E864/E878 data are shown as most probable values with the 98% confidence level of the minimum value indicated by the lower error bar. Upper limits are not given horizontal bar indicate the bin widths.

At present there is no explanation for the large value of the $\bar\Lambda/\bar p$-ratio for central events, nor the strong centrality dependence of this quantity.

Two Particle Correlations

Applying the Hanbury-Brown Twiss analysis to correlation between identical particles is an important tool for studying the size and possibly the shape of the hot fireball, from which these particles are emitted, provided certain conditions are fulfilled. We are applying this type of analysis to pairs of $\pi^+\pi^+$ and $\pi^-\pi^-$ pairs from Au - Au collisions at 6, 8, and 10.8 GeV/nucleon. If sufficient data are available this analysis will also be applied to pion-pairs emitted at specific azimuthal angular bins relative to the reaction

plane in order to attempt to determine possible non-spherical momenta of the fireball and/or shadowing effects of the spectators. Preliminary results from this analysis was published in conference proceedings.[11] This work will also constitute the Ph.D. thesis for Burt Holzman, University of Illinois at Chicago.

*University of Illinois at Chicago, †Brookhaven National Laboratory, ‡University of California at Riverside, §Massachusetts Institute of Technology, ¶Yonsei University, Seoul, Korea, ||University of Maryland, **University of Rochester, ††Columbia University

1L. Ahle *et al*., Phys. Lett. **B476**, 1 (2000).
2L. Ahle *et al*., Phys. Lett. **B490**, 53 (2000).
3B. B. Back *et al*., J. Phys. G **27**, 301 (2001).
4B. B. Back *et al*., Phys. Rev. Lett. **86**, 1970 (2001).
5B. B. Back *et al*., submitted to Phys. Rev. Lett. (2001).
6J. Rafelski and B. Muller, Phys. Rev. Lett. **48**, 1066 (1982); erratum Phys. Rev. Lett. **56**, 2334 (1982).
7J. Rafelski, Phys. Rep. **88**, 331 (1982).
8P. Koch, B. Mueller, and J. Rafelski, Phys. Rep. **142**, 167 (1986).
9J. Rafelski, M. Danos, Phys. Rev. C **50**, 1684 (1994).
10F. Beccatini *et al*., hep-ph/0002267. The $\bar{\Lambda}/\bar{p}$-ratio is estimated here by assuming the calculated yield of K^+, multiplying quoted ratios and correcting for Λ-feed-down.
11Burt Holzman *et al*. "Advances in Nuclear Dynamics 5", Plenum Press, New York, 1999, Eds. Bauer and Westfall, p. 189.